International Journal of Solids and Structures 193–194 (2020) 328–337

Contents lists available at ScienceDirect

International Journal of Solids and Structures

journal homepage: www.elsevier.com/locate/ijsolstr

A 3-dimensional elastic beam model for form-finding of bending-active gridshells

Yusuke Sakai[a,*], Makoto Ohsaki[b], Sigrid Adriaenssens[c]

[a] Department of Architecture and Architectural Engineering, Kyoto University, Kyoto-Daigaku Katsura, Nishikyo, Kyoto 615-8540, Japan
[b] Department of Architecture and Architectural Engineering, Kyoto University, Japan
[c] Department of Civil & Environmental Engineering, Princeton University, USA

ARTICLE INFO

Article history:
Received 1 August 2019
Revised 6 February 2020
Accepted 18 February 2020
Available online 21 February 2020

Keywords:
Elastic gridshell
Dynamic relaxation method
FEM
Bending-active structure
Large-deformation analysis

ABSTRACT

In this paper, we present a 3-dimensional elastic beam model for the form-finding and analysis of elastic gridshells subjected to bending deformation at the self-equilibrium state. Although the axial, bending, and torsional strains of the beam elements are small, the curved beams connected by hinge joints are subjected to large-deformation. The directions and rotation angles of the unit normal vectors at the nodes of the curved surfaces in addition to the translational displacements are chosen as variables. Based on the 3-dimensional elastic beam model, deformation of an element is derived from only the local geometrical relations between the orientations of elements and the unit normal vectors at nodes without resorting to a large rotation formulation in the 3-dimensional space. Deformation of a gridshell with hinge joints is also modeled using the unit normal vectors of the surface. An energy-based formulation is used for deriving the residual forces at the nodes, and the proposed model is implemented within dynamic relaxation method for form-finding and analysis of gridshells. The accuracy of the proposed method using dynamic relaxation method is confirmed in comparison to the results by finite element analysis. The results are also compared with those by optimization approach for minimizing the total potential energy derived using the proposed formulation.

1. Introduction

Single-layer latticed shells with quadrilateral units can be generated by bending and connecting long beams. Such latticed shells are called gridshells (Adriaenssens et al., 2004; Happold and Liddell, 1975; Harris et al., 2003; Sakai and Ohsaki, 2018). We consider the form-finding of gridshells composed of actively-bent slender beams connected by hinge joints. The curved shape of a gridshell is generated from a flat grid of interconnected straight unstressed beams. During the construction process, forced displacements are given at the boundary, and the flexible members are deformed to obtain a desired shape. Since the equilibrium shape of a curved surface is significantly different from the initial flat shape, a large-deformation analysis should be carried out iteratively to obtain the shape desired by the designer. However, sophisticated software packages such as Abaqus (Systèmes, 2016) are not available to general structural designers; therefore, some simple algorithms are needed for use in the process of structural design.

D'Amico et al. (2016) investigated the features of implicit and explicit integration methods for large-deformation analysis of bending-active structures. Implicit integration method, such as Newmark-β method, takes advantage of the numerical stability; however, Newton iterations are needed for obtaining the responses at the next incremental step, and accordingly, substantial computational cost is needed for a highly-nonlinear large-scale structure. Because we are interested in the final self-equilibrium shape obtained by large deformation analysis, and as the equilibrium shape at the intermediate state between the flat shape and the curved final shape is of no importance, implicit integration methods are not effective due to their large computational cost.

On the other hand, explicit integration methods, such as the dynamic relaxation method (DRM) (Day, 1965), can derive the responses at the next incremental step explicitly from the responses at the current step only; therefore, no Newton iteration is needed. This property enables us to implement the algorithm in a simple manner. The DRM converts the static analysis problem

* Corresponding author.
E-mail address: sakai.yusuke.52v@st.kyoto-u.ac.jp (Y. Sakai).

https://doi.org/10.1016/j.ijsolstr.2020.02.034

to a dynamic problem, and solves it using explicit integration. The DRM is widely used for form-finding of elastic gridshells (Lázaro et al., 2018), because only the final static equilibrium state is needed. Another merit of using the DRM is that it does not require derivation of the tangent stiffness matrix, and utilizes only the internal forces for computation of the unbalanced loads.

Many large-deformation analysis methods of gridshells have been developed for practical tools. Lázaro et al. (2018) noted that a rigorous definition of the beam element is essential for implementing the DRM for a 3-dimensional form-finding problem. Two types of discretization, i.e., finite-difference and finite-element, have been proposed. Each beam element defined by finite-difference discretization is composed of the two end nodes and the center node. We can compute the curvatures (strains) at the center node with the geometrical relationship among the three nodes, and derive the shear forces and the bending moments at each node. Degrees of freedom (DOFs) at each node are three (D'Amico et al., 2016; Barnes et al., 2013; Adriaenssens and Barnes, 2001) or four (Lefevre et al., 2017). The 3DOF node can represent only the translational displacements, while the 4DOF node also includes the torsional displacement.

Finite-element discretization describes a beam element consisting of two end nodes, which have six DOFs at each node representing three translational and three rotational displacements. This kind of discretization usually takes advantages of the co-rotational formulation (Belytschko and Hsieh, 1973; Crisfield, 1990; Krenk, 2009; Li and Vu-Quoc, 2010; Hsiao, 1992; Simo and Vu-Quoc, 1991), which enables us to obtain the equilibrium shape of a deformed flexible beam by nodal locations and the directions of local axes under assumption of large displacement-small strain. The co-rotational formulation has been implemented to the DRM in (D'Amico et al., 2014; 2015; Li and Knippers, 2012; Senatore and Piker, 2015).

A geometrically exact rod model was proposed by Reissner (1972) and improved by Simo (1985) and Simo and Vu-Quoc (1986). Furthermore, the beam elements have successfully been applied to geometrically nonlinear analysis (Cardona and Géradin, 1988; Ibrahimbegović, 1995; Sonneville et al., 2014). Bessini et al. (2017) proposed a method to implement the geometrically exact rod model into the DRM. The model also has six DOFs at each node representing the translational and rotational displacements. The particular merit of the geometrically exact rod model is that it can describe the exact locations and rotations of cross-sections of slender beams subjected to large deformation, using a mathematically exact formulation. However, it may be too complicated for the form-finding of gridshells.

Rombouts et al. (2019) proposed a form-finding and optimization method of gridshells using co-rotational formulation implemented to an implicit DRM (Rombouts et al., 2018). The implicit DRM may be faster than an explicit DRM to obtain the curved final shape, because fewer steps are needed before reaching convergence. However, the implicit DRM is based on the nonlinear iterative solution technique that requires the tangent stiffness matrix of the nonlinear system at each incremental step.

In this paper, we propose an energy-based formulation for 3-dimensional beam model for large-deformation analysis of a gridshell specifically using the DRM based on the assumption of large displacement-small strain. The concept of our beam element is based on the co-rotating beam element, which is explained and illustrated in Krenk (2009). However, our method has the following novelty. The unit normal vector perpendicular to the tangent plane of a curved surface at the deformed state is assigned at each end node of a beam element and used for defining the local coordinates. In this way, the deformed state is uniquely defined by the nodal locations and the surface normal vectors. The two components of normal vector as well as the rotation around the normal vector are used as independent variables to avoid additional constraints assigned in Nielsen and Krenk (2014). The residual forces are derived by differentiating the total potential energy for use in the DRM, which is an explicit integration method. The method based on direct minimization of the total potential energy by solving an unconstrained optimization problem is also presented for comparison to the DRM. Furthermore, a hinge at node can be naturally incorporated by allowing the two intersecting beams have two independent rotations around the surface normal vector. Accuracy of the proposed method is verified in the numerical examples of gridshells in comparison to the results obtained by a finite element analysis (FEM) package and those by directly minimizing the total potential energy using an optimization algorithm.

2. Dynamic relaxation method

DRM is an explicit integration method for dynamically solving static problems of structures. The method has been proposed by Day (1965) and applied to form-finding of flexible structures such as membrane structures, cable nets (Bel Hadj Ali et al., 2017), tensegrity structures (Bel Hadj Ali et al., 2011), and bending-active structures. The main schematic of the DRM is to utilize the nodal displacements for modeling the configurations of structures and trace the motions of the nodes incrementally. The artificial kinetic damping makes the motions converge to the static equilibrium state.

Consider a geometrically nonlinear structure discretized into beam elements. Let $\boldsymbol{a}$, $\boldsymbol{v}$, $\boldsymbol{r}$, $\boldsymbol{x}$, and $\boldsymbol{u}$ denote the vectors containing the acceleration, the velocity, the internal restoring force, the nodal coordinate, and the displacement, respectively, of all degrees of freedom of the structure. The mass matrix is denoted by $\boldsymbol{M}$. In our method, the damping matrix is omitted, because we use the kinetic damping explained in Step 6 of the following algorithm of DRM. Since these matrices are diagonal, the equations below can be formulated at each node, or even for each displacement component. However, the vectors and the matrices with the size of total degrees of freedom is used to derive the simple formulation of the residual forces in Section 4. Motions of the nodes under existence of the static external force vector $\boldsymbol{p}$ are computed from the following equations of motion:

$$\boldsymbol{M}\boldsymbol{a} + \boldsymbol{r} = \boldsymbol{p}. \tag{1}$$

Eq. (1) represents a nonlinear static equilibrium equation, if both $\boldsymbol{a}$ and $\boldsymbol{v}$ are $\boldsymbol{0}$. The vector of residual forces of static equilibrium at the current time t is denoted by $\boldsymbol{R}^t$, which is written as

$$\boldsymbol{R}^t = -\boldsymbol{r}^t + \boldsymbol{p}. \tag{2}$$

In the following, the superscript t denotes the value at time t. Eq. (1) can be rewritten using $\boldsymbol{R}^t$ as

$$\boldsymbol{M}\boldsymbol{a}^t = \boldsymbol{R}^t. \tag{3}$$

The kinetic energy K is defined as

$$K = \frac{1}{2}\boldsymbol{v}^T\boldsymbol{M}\boldsymbol{v}. \tag{4}$$

The convergence criterion is specified so that the norm of the residual force vector is less than the specified value, which indicates that a static equilibrium is achieved.

The algorithm of DRM is summarized as follows:

Algorithm of DRM:

Step 1: Assign the initial time increment $\Delta t = \Delta t_{\mathrm{ini}}$, and set initial nodal location vector as $\boldsymbol{x} = \bar{\boldsymbol{x}}$. Set the initial conditions at $t = 0$ for displacements and velocities as $\boldsymbol{u}^t = \boldsymbol{0}$ and $\boldsymbol{v}^{t-\Delta t/2} = \boldsymbol{0}$, respectively, and initialize the kinetic energy as $K^{t-\Delta t/2} = 0$.

Step 2: Compute the residual forces $\boldsymbol{R}^t$ from Eq. (2).

Step 3: Using Eq. (3), compute $\boldsymbol{a}^t$ as

$$\boldsymbol{a}^t = \boldsymbol{M}^{-1}\boldsymbol{R}^t. \tag{5}$$

Note that the inverse of mass matrix is not actually computed. The mass matrix is diagonal, and each component of acceleration is updated independently using Eq. (5).

Step 4: Update the vectors of velocity, displacement, and nodal location as:

$$\boldsymbol{v}^{t+\Delta t/2} = \boldsymbol{v}^{t-\Delta t/2} + \Delta t\boldsymbol{a}^t, \tag{6}$$

$$\boldsymbol{u}^{t+\Delta t} = \boldsymbol{u}^t + \Delta t\boldsymbol{v}^{t+\Delta t/2}, \tag{7}$$

$$\boldsymbol{x}^{t+\Delta t} = \bar{\boldsymbol{x}} + \boldsymbol{u}^{t+\Delta t}. \tag{8}$$

Step 5: Compute the kinetic energy $K^{t+\Delta t/2}$ from Eq. (4).

Step 6: If the inequality

$$K^{t-\Delta t/2} \geq K^{t+\Delta t/2} \tag{9}$$

is satisfied, go to Step 7; otherwise, update the time as $t \leftarrow t + \Delta t$, and go to Step 2.

Step 7: Terminate the algorithm, if the convergence criterion with respect to the residual forces $\boldsymbol{R}^{t+\Delta t}$ is satisfied. Otherwise, reset the velocity vector as $\boldsymbol{v}^{t+\Delta t/2} = \boldsymbol{0}$, multiply the time interval Δt using the specified parameter ξ as $\Delta t \leftarrow \xi\Delta t$, update the time as $t \leftarrow t + \Delta t$, and then go to Step 2. We use the parameter $\xi (0 < \xi < 1)$ so that the time step Δt can initially have a large value to reduce the computational cost, and can be decreased to improve the accuracy of the solution as the deformation converges to the static equilibrium solution.

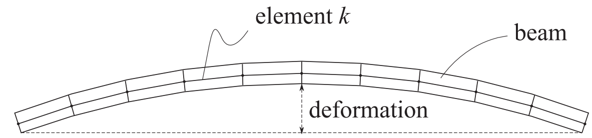

Fig. 1. Form of beam with large deformation and small strains.

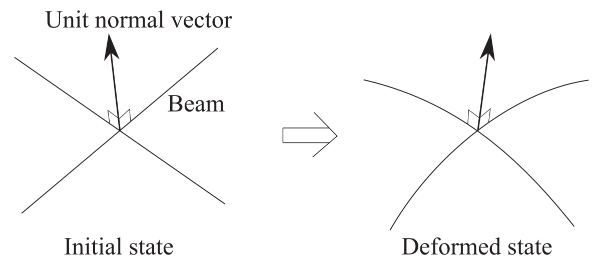

Fig. 2. Deformed unit normal vector generated from a grid composed of beams.

3. Formulation of 3-dimensional elastic beam element model

A geometrically nonlinear energy-based formulation for the 3-dimensional elastic beam element is proposed for application to DRM. The beam of a gridshell is discretized into several elements as shown in Fig. 1, and the conventional assumption of large displacement-small strain is used; i.e., the nodal displacements are large, but the axial and bending strains in each element are sufficiently small.

3.1. Local basis vectors and rotational displacements at nodes

A 3-dimensional Euler-Bernoulli beam element is generally composed of two end nodes, each of which has three translational and three rotational displacement components as independent variables. The local basis vectors are usually used to express magnitude of the rotational deformation (D'Amico et al., 2014; 2015; Li and Knippers, 2012; Senatore and Piker, 2015; Krenk, 2009; Nielsen and Krenk, 2014). In the formulation proposed in this paper, the rotational displacements are derived from the unit normal vectors at nodes, as shown in Fig. 2, which are orthogonal to the two curved lines of intersecting beams after deformation. The two projected components of nodal unit normal vector are used to formulate torsion and one component of bending. The other component of bending is expressed by rotation along its axis.

Fig. 3(a) shows element k connecting nodes j and $j+1$. The local basis vector directed from node j to node $j+1$ is denoted by $\hat{\boldsymbol{t}}_{1,k}$. The coordinate vector and the unit normal vector of the surface at node j are denoted by $\boldsymbol{X}_j$ and $\hat{\boldsymbol{n}}_j$, respectively. Throughout the paper, we use the notation $\hat{(\cdot)}$ for a unit vector. Using the unit vector $\hat{\boldsymbol{r}}_k$ of element k, which is defined as the average of the normal vectors at nodes j and $j+1$, the basis vectors $\hat{\boldsymbol{t}}_{1,k}$, $\hat{\boldsymbol{t}}_{2,k}$, and $\hat{\boldsymbol{t}}_{3,k}$ are defined by the following equations:

$$\hat{\boldsymbol{t}}_{1,k} = \frac{\boldsymbol{X}_{j+1} - \boldsymbol{X}_j}{||\boldsymbol{X}_{j+1} - \boldsymbol{X}_j||}, \tag{10}$$

$$\hat{\boldsymbol{t}}_{2,k} = \frac{\hat{\boldsymbol{r}}_k \times \hat{\boldsymbol{t}}_{1,k}}{||\hat{\boldsymbol{r}}_k \times \hat{\boldsymbol{t}}_{1,k}||}, \tag{11}$$

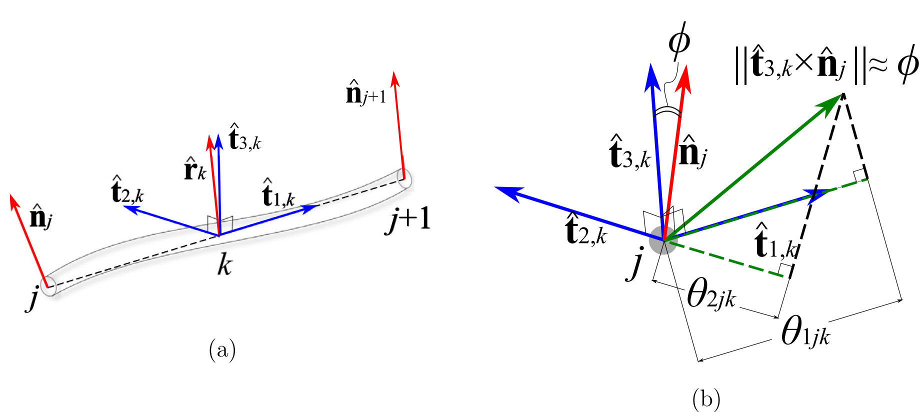

Fig. 3. Definitions of local basis vectors and rotational displacements of element k connecting nodes j and $j+1$; (a) local basis vectors $\hat{\boldsymbol{t}}_{1,k}$, $\hat{\boldsymbol{t}}_{2,k}$, and $\hat{\boldsymbol{t}}_{3,k}$ of element k, (b) rotational displacements θ_{1jk} and θ_{2jk} derived from the geometrical relationship of the unit vectors at node j.

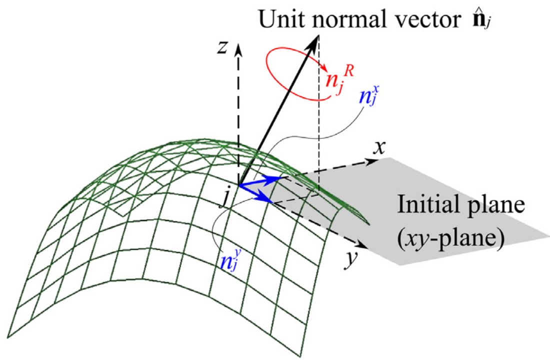

Fig. 4. Projected components of $\hat{\boldsymbol{n}}_j$.

$$\hat{\boldsymbol{t}}_{3,k} = \frac{\hat{\boldsymbol{t}}_{1,k} \times \hat{\boldsymbol{t}}_{2,k}}{||\hat{\boldsymbol{t}}_{1,k} \times \hat{\boldsymbol{t}}_{2,k}||}, \tag{12}$$

$$\hat{\boldsymbol{r}}_k = \frac{\hat{\boldsymbol{n}}_j + \hat{\boldsymbol{n}}_{j+1}}{||\hat{\boldsymbol{n}}_j + \hat{\boldsymbol{n}}_{j+1}||}. \tag{13}$$

The rotational displacements at node j of element k around the basis vectors $\hat{\boldsymbol{t}}_{1,k}$ and $\hat{\boldsymbol{t}}_{2,k}$ are denoted by θ_{1jk} and θ_{2jk}, respectively, as shown in Fig. 3(b). The norm of the cross product $\hat{\boldsymbol{t}}_{3,k} \times \hat{\boldsymbol{n}}_j$ is regarded as the local rotation angle ϕ at node j in the plane perpendicular to $\hat{\boldsymbol{n}}_j$, because the norms of $\hat{\boldsymbol{t}}_{3,k}$ and $\hat{\boldsymbol{n}}_j$ are equal to 1. Therefore, we can obtain the rotational displacements around $\hat{\boldsymbol{t}}_{1,k}$, $\hat{\boldsymbol{t}}_{2,k}$ as (Krenk, 2009)

$$\theta_{1jk} = \hat{\boldsymbol{t}}_{1,k} \cdot \left(\hat{\boldsymbol{t}}_{3,k} \times \hat{\boldsymbol{n}}_j\right), \tag{14}$$

$$\theta_{2jk} = \hat{\boldsymbol{t}}_{2,k} \cdot \left(\hat{\boldsymbol{t}}_{3,k} \times \hat{\boldsymbol{n}}_j\right). \tag{15}$$

Suppose the gridshell is initially on xy-plane of the global coordinates (x, y, z). Fig. 4 shows the two projection components n_j^x and n_j^y of $\hat{\boldsymbol{n}}_j = [n_j^x, n_j^y, n_j^z]^T$ onto xy-plane. At the initial state of the grid on xy-plane, the components of $\hat{\boldsymbol{n}}_j$ are given as $[0, 0, 1]^T$. In the numerical examples of DRM in Section 6, bounds are not assigned for n_j^x and n_j^y, while n_j^z is positive at all nodes. Thus, the components of $\hat{\boldsymbol{n}}_j$ at a deformed state are computed as

$$\hat{\boldsymbol{n}}_j = \begin{cases} \left[\dfrac{n_j^x}{\sqrt{n_j^{x2}+n_j^{y2}}}, \dfrac{n_j^y}{\sqrt{n_j^{x2}+n_j^{y2}}}, 0\right]^T & \text{for} \;\; n_j^{x2}+n_j^{y2} > 1 \\ \left[n_j^x, n_j^y, \sqrt{1-\left(n_j^{x2}+n_j^{y2}\right)}\right]^T & \text{for} \;\; n_j^{x2}+n_j^{y2} \le 1 \end{cases}. \tag{16}$$

Finally, let n_j^R denote the rotation around $\hat{\boldsymbol{n}}_j$. Then $\theta_{3jk} = n_j^R$ is chosen as the third independent rotational displacement component.

3.2. Continuity of rotation at internal nodes

When multiple beam elements are rigidly connected to node j as shown in Fig. 5(a), there is only one independent rotational displacement at node j around the normal vector of the surface. Suppose the rotation n_j^R of element k is chosen as the independent rotational displacement variable, and elements k and $k+1$ are connected to node j. Let α denote the projected angle between elements k and $k+1$ at node j. The dependent variable $\theta_{3j(k+1)}$ is computed from n_j^R using the following algorithm:

Step 1: Project $\hat{\boldsymbol{t}}_{1,k}$ onto a plane perpendicular to $\hat{\boldsymbol{n}}_j$ to obtain the vector $\boldsymbol{f}_1$.
Step 2: Normalize $\boldsymbol{f}_1$ as $\hat{\boldsymbol{f}}_1 = \boldsymbol{f}_1/||\boldsymbol{f}_1||$.
Step 3: Compute $\hat{\boldsymbol{f}}_2$ by rotating $\hat{\boldsymbol{f}}_1$ by the angle $n_j^R + \alpha$ around $\hat{\boldsymbol{n}}_j$.
Step 4: Compute the cross product $\boldsymbol{f}_3 = \hat{\boldsymbol{t}}_{1,k+1} \times \hat{\boldsymbol{f}}_2$, and obtain $\theta_{3j(k+1)}$ as the component of $\boldsymbol{f}_3$ in the direction of $\hat{\boldsymbol{n}}_j$.

The details of algorithm are described below.

First, $\boldsymbol{f}_1$ is defined, as follows, as the basis vector $\hat{\boldsymbol{t}}_{1,k}$ projected to the tangent plane at node j as shown in Fig. 5(a):

$$\boldsymbol{f}_1 = \hat{\boldsymbol{t}}_{1,k} - \left(\hat{\boldsymbol{t}}_{1,k} \cdot \hat{\boldsymbol{n}}_j\right)\hat{\boldsymbol{n}}_j. \tag{17}$$

In this plane, we rotate the normalized vector $\hat{\boldsymbol{f}}_1 = \boldsymbol{f}_1/||\boldsymbol{f}_1||$ around $\hat{\boldsymbol{n}}_j$. The angle $n_j^R + \alpha$ in Step 3 represents the sum of the nodal rotation $n_j^R = \theta_{3jk}$ obtained from the deformation of element k and the initial angle α between the elements. In other words, the direction of element k at node j is found by rotating by the angle

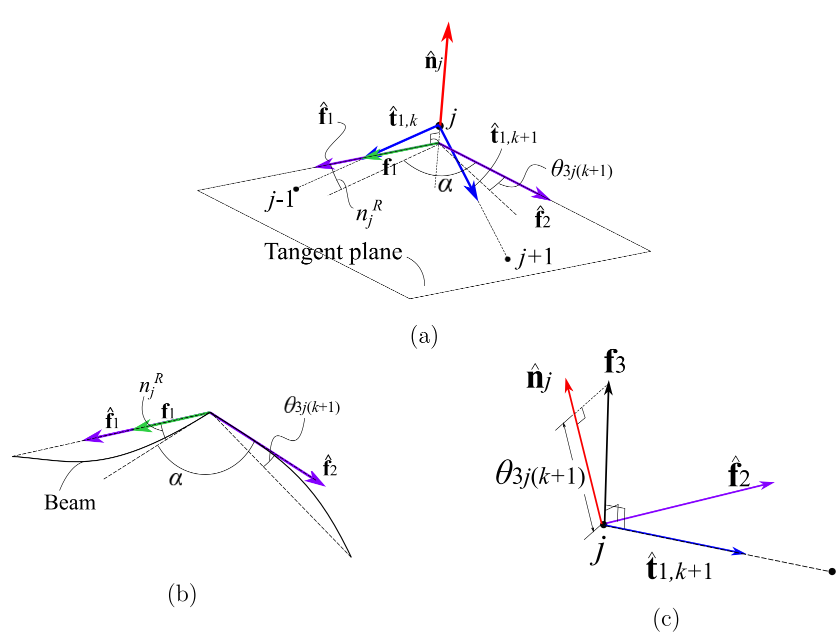

Fig. 5. Computation of the dependent rotational displacement around unit normal vector at node j; (a) Step 1-3 (Isometric), (b) Step 1-3 (Tangent plane), (c) Step 4.

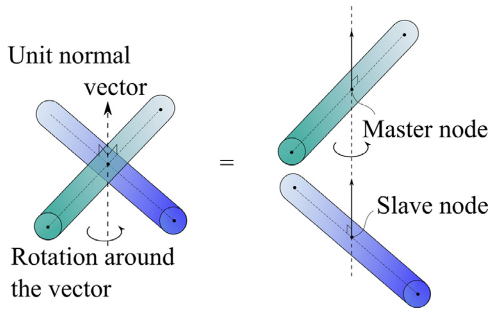

Fig. 6. Illustration of the hinge joint model using shared unit normal vector under large deformation.

θ_{3jk}, and the direction of element $k+1$ is found by further rotating by the angle α. The vector $\hat{\boldsymbol{f}}_2$ in Fig. 5(b) shows the projected tangential direction of element $k+1$ at node j at the deformed state. Therefore, $\hat{\boldsymbol{f}}_2$ is obtained by rotating $\hat{\boldsymbol{f}}_1$ around $\hat{\boldsymbol{n}}_j$ as

$$\hat{\boldsymbol{f}}_2 = \hat{\boldsymbol{f}}_1 \cos\left(n_j^R + \alpha\right) + \left(\hat{\boldsymbol{n}}_j \times \hat{\boldsymbol{f}}_1\right) \sin\left(n_j^R + \alpha\right). \tag{18}$$

Process of Step 4 is illustrated in Fig. 5(c). The component of cross product $\boldsymbol{f}_3 = \hat{\boldsymbol{t}}_{1,k+1} \times \hat{\boldsymbol{f}}_2$ projected to $\hat{\boldsymbol{n}}_j$ is equal to the rotation angle $\theta_{3j(k+1)}$ of element $k+1$ at node j around $\hat{\boldsymbol{n}}_j$ as

$$\theta_{3j(k+1)} = \boldsymbol{f}_3 \cdot \hat{\boldsymbol{n}}_j. \tag{19}$$

3.3. Rigid support condition and hinge joint model

A rotational boundary condition at a fixed support is assigned in the following manner. Consider element k connecting a fixed support j and a free node $j+1$. The basis vectors in the member directions at undeformed and deformed states are denoted by $\hat{\boldsymbol{t}}^*_{1,k}$ and $\hat{\boldsymbol{t}}_{1,k}$, respectively. We compute the cross product of these vectors as

$$\boldsymbol{g}_1 = \hat{\boldsymbol{t}}_{1,k} \times \hat{\boldsymbol{t}}^*_{1,k} \tag{20}$$

which represents the vector of local rotational displacement at node j. Finally, the rotational displacement of member k around unit normal vector $\hat{\boldsymbol{n}}_j$ is computed as

$$\theta_{3jk} = \boldsymbol{g}_1 \cdot \hat{\boldsymbol{n}}_j, \tag{21}$$

and the rotation n_j^R at the fixed node is constrained as

$$n_j^R = \theta_{3jk}. \tag{22}$$

The curved beams of gridshell are generally connected by hinge joints. A pair of beams can rotate with different angles around the axis of hinge, which is in the direction of unit normal vector of the surface as shown in Fig. 6. In our model, the two overlapping nodes at a hinge joint are classified into the master node and the slave node. The master node has six DOFs, and the translational and rotational displacements of the slave node are the same as those of the master node except the rotation around the unit normal vector of the surface; thus, the slave node has only one DOF, and the forces in three directions and the moments except the bending moment around the hinge are transmitted by a hinge joint.

3.4. Total potential energy

The total potential energy is formulated here to differentiate it with respect to the displacement components and obtain the residual force vector. Let E and G denote Young's modulus and the shear modulus of the beam, respectively. The cross-sectional area and the torsional constant are denoted by A and J, respectively.

We consider sections with two axes of symmetry. The unit normal vector $\hat{\boldsymbol{n}}_j$ is directed to one of the principal axes of the section of each element connected to the node. Since the assumption of small deformation is used for each beam element, we can assume the vectors $\hat{\boldsymbol{t}}_{2,k}$ and $\hat{\boldsymbol{t}}_{3,k}$ are directed to the two principal axes of element k, for which the second moment of areas are denoted by I_{2k} and I_{3k}, respectively.

The locations of node j at the initial and deformed states are denoted by $(\bar{X}_j^x, \bar{X}_j^y, \bar{X}_j^z)^T$ and $(X_j^x, X_j^y, X_j^z)^T$, respectively, with the nodal loads $\boldsymbol{P}_j$. The displacement vector of node j is denoted by $(U_j^x, U_j^y, U_j^z)^T = (X_j^x, X_j^y, X_j^z)^T - (\bar{X}_j^x, \bar{X}_j^y, \bar{X}_j^z)^T$. The elongation e_k of element k is computed from the element length L_k at the deformed state and the initial length $\bar{L}_k$. Then, the total potential energy Π_{total} of the gridshell, which has m members and s free nodes, is obtained from the internal strain energy and the external work as

$$\Pi_{\mathrm{total}} = \sum_{k=1}^{m} \Pi_{\mathrm{int}}^k - \sum_{j=1}^{s} \Pi_{\mathrm{ext}}^j, \tag{23}$$

$$\begin{aligned}\Pi_{\mathrm{int}}^k = {} & \frac{EA}{2\bar{L}_k} {e_k}^2 + \frac{GJ}{2\bar{L}_k}\left(\theta_{1(j+1)k} - \theta_{1jk}\right)^2 \\ & + \frac{EI_{2k}}{2\bar{L}_k}\left[4\left(\theta_{2jk}\right)^2 + 4\theta_{2jk}\theta_{2(j+1)k} + 4\left(\theta_{2(j+1)k}\right)^2\right] \\ & + \frac{EI_{3k}}{2\bar{L}_k}\left[4\left(\theta_{3jk}\right)^2 + 4\theta_{3jk}\theta_{3(j+1)k} + 4\left(\theta_{3(j+1)k}\right)^2\right],\end{aligned} \tag{24}$$

$$\Pi_{\mathrm{ext}}^j = \boldsymbol{P}_j \cdot \begin{bmatrix} X_j^x - \bar{X}_j^x \\ X_j^y - \bar{X}_j^y \\ X_j^z - \bar{X}_j^z \end{bmatrix} = \boldsymbol{P}_j \cdot \begin{bmatrix} U_j^x \\ U_j^y \\ U_j^z \end{bmatrix}, \tag{25}$$

where Π_{int}^k is the internal strain energy of element k connecting nodes j and $j+1$, and Π_{ext}^j is the external work at node j. The complementary energy formulations of the internal strain energy in Eqs. (23) and (24) are based on the small strains corresponding to small local rotations at member ends (Krenk, 2009). Furthermore, the form of bending strain energy is derived from the following expression of the bending moments B_1 and B_2 at member ends using bending stiffness matrix:

$$\begin{bmatrix} B_1 \\ B_2 \end{bmatrix} = \frac{EI_{ik}}{\bar{L}_k}\begin{bmatrix} 2 & 1 \\ 1 & 2 \end{bmatrix}\begin{bmatrix} \theta_{ijk} \\ \theta_{i(j+1)k} \end{bmatrix}, \qquad i = \{2, 3\}. \tag{26}$$

4. Residual forces

The residual forces are defined in Eq. (2) as the difference between the internal and external forces. Let b_i denote the ith component of a vector $\boldsymbol{b}$. The residual force corresponding to the ith degree of freedom is obtained by differentiating the internal strain energy and the external work with respect to the ith component u_i of the displacement vector $\boldsymbol{u}$ as

$$\begin{aligned} R_i^t &= -r_i^t + p_i \\ &= -\sum_{k=1}^{m} \frac{\partial \Pi_{\mathrm{int}}^k}{\partial u_i} + \sum_{j=1}^{s} \frac{\partial \Pi_{\mathrm{ext}}^j}{\partial u_i}. \end{aligned} \tag{27}$$

Furthermore, in the numerical examples, a sensitivity analysis is used for finding the equilibrium shape by solving an optimization problem. Therefore, we derive the differential coefficients of the strain energy and the external work with respect to the displacement variables next.

Taking the partial derivatives of Eqs. (24) and (25) with respect to u_i, which represents displacement variable such as U_j^x, U_j^y, U_j^z,

n_j^x, n_j^y, and n_j^R, the differential coefficients are obtained as

$$\begin{aligned}\frac{\partial \Pi_{\text{int}}^k}{\partial u_i} &= \frac{EA}{\bar{L}_k} e_k \frac{\partial e_k}{\partial u_i} + \frac{GJ}{\bar{L}_k}\left(\theta_{1(j+1)k} - \theta_{1jk}\right)\frac{\partial\left(\theta_{1(j+1)k} - \theta_{1jk}\right)}{\partial u_i} \\ &+ \frac{2EI_{2k}}{\bar{L}_k}\left(\frac{2\partial\theta_{2jk}}{\partial u_i}\theta_{2jk} + \frac{\partial\theta_{2(j+1)k}}{\partial u_i}\theta_{2jk} \right. \\ &\left. + \frac{\partial\theta_{2jk}}{\partial u_i}\theta_{2(j+1)k} + \frac{2\partial\theta_{2(j+1)k}}{\partial u_i}\theta_{2(j+1)k}\right) \\ &+ \frac{2EI_{3k}}{\bar{L}_k}\left(\frac{2\partial\theta_{3jk}}{\partial u_i}\theta_{3jk} + \frac{\partial\theta_{3(j+1)k}}{\partial u_i}\theta_{3jk} \right. \\ &\left. + \frac{\partial\theta_{3jk}}{\partial u_i}\theta_{3(j+1)k} + \frac{2\partial\theta_{3(j+1)k}}{\partial u_i}\theta_{3(j+1)k}\right), \end{aligned} \tag{28}$$

$$\frac{\partial \Pi_{\text{ext}}^j}{\partial u_i} = \boldsymbol{P}_j \cdot \begin{bmatrix} \frac{\partial U_j^x}{\partial u_i} \\ \frac{\partial U_j^y}{\partial u_i} \\ \frac{\partial U_j^z}{\partial u_i} \end{bmatrix}. \tag{29}$$

Derivative of the axial deformation is equal to that of the length of the deformed element as

$$\frac{\partial e_k}{\partial u_i} = \frac{\partial\left(L_k - \bar{L}_k\right)}{\partial u_i} = \frac{\partial L_k}{\partial u_i} \tag{30}$$

which is obtained as

$$\frac{\partial L_k}{\partial u_i} = \frac{1}{L_k}\left[X_{j+1}^x - X_j^x,\quad X_{j+1}^y - X_j^y,\quad X_{j+1}^z - X_j^z\right]\begin{bmatrix} \frac{\partial\left(U_{j+1}^x - U_j^x\right)}{\partial u_i} \\ \frac{\partial\left(U_{j+1}^y - U_j^y\right)}{\partial u_i} \\ \frac{\partial\left(U_{j+1}^z - U_j^z\right)}{\partial u_i} \end{bmatrix}. \tag{31}$$

To compute the differential coefficients of the rotational displacements, differentiate Eqs. (14) and (15) with respect to u_i as

$$\begin{aligned}\frac{\partial\theta_{1jk}}{\partial u_i} &= \frac{\partial}{\partial u_i}\left[\hat{\boldsymbol{t}}_{1,k}\cdot\left(\hat{\boldsymbol{t}}_{3,k}\times\hat{\boldsymbol{n}}_j\right)\right] \\ &= \frac{\partial\hat{\boldsymbol{t}}_{1,k}}{\partial u_i}\cdot\left(\hat{\boldsymbol{t}}_{3,k}\times\hat{\boldsymbol{n}}_j\right) + \hat{\boldsymbol{t}}_{1,k}\cdot\left(\frac{\partial\hat{\boldsymbol{t}}_{3,k}}{\partial u_i}\times\hat{\boldsymbol{n}}_j + \hat{\boldsymbol{t}}_{3,k}\times\frac{\partial\hat{\boldsymbol{n}}_j}{\partial u_i}\right),\end{aligned} \tag{32}$$

$$\begin{aligned}\frac{\partial\theta_{2jk}}{\partial u_i} &= \frac{\partial}{\partial u_i}\left[\hat{\boldsymbol{t}}_{2,k}\cdot\left(\hat{\boldsymbol{t}}_{3,k}\times\hat{\boldsymbol{n}}_j\right)\right] \\ &= \frac{\partial\hat{\boldsymbol{t}}_{2,k}}{\partial u_i}\cdot\left(\hat{\boldsymbol{t}}_{3,k}\times\hat{\boldsymbol{n}}_j\right) + \hat{\boldsymbol{t}}_{2,k}\cdot\left(\frac{\partial\hat{\boldsymbol{t}}_{3,k}}{\partial u_i}\times\hat{\boldsymbol{n}}_j + \hat{\boldsymbol{t}}_{3,k}\times\frac{\partial\hat{\boldsymbol{n}}_j}{\partial u_i}\right).\end{aligned} \tag{33}$$

Differential coefficients of $\hat{\boldsymbol{n}}_j$ are expressed from Eq. (16) as

$$\frac{\partial\hat{\boldsymbol{n}}_j}{\partial u_i} = \begin{cases} \begin{bmatrix} \frac{\partial n_j^x}{\partial u_i}\frac{1}{\sqrt{n_j^{x2}+n_j^{y2}}} - \frac{n_j^x}{\left(n_j^{x2}+n_j^{y2}\right)^{3/2}}\left(\frac{\partial n_j^x}{\partial u_i}n_j^x + \frac{\partial n_j^y}{\partial u_i}n_j^y\right) \\ \frac{\partial n_j^y}{\partial u_i}\frac{1}{\sqrt{n_j^{x2}+n_j^{y2}}} - \frac{n_j^y}{\left(n_j^{x2}+n_j^{y2}\right)^{3/2}}\left(\frac{\partial n_j^x}{\partial u_i}n_j^x + \frac{\partial n_j^y}{\partial u_i}n_j^y\right) \\ 0 \end{bmatrix} & \text{for } n_j^{x2}+n_j^{y2} > 1 \\ \begin{bmatrix} \frac{\partial n_j^x}{\partial u_i} \\ \frac{\partial n_j^y}{\partial u_i} \\ -\frac{\frac{\partial n_j^x}{\partial u_i}n_j^x + \frac{\partial n_j^y}{\partial u_i}n_j^y}{\sqrt{1-\left(n_j^{x2}+n_j^{y2}\right)}} \end{bmatrix} & \text{for } n_j^{x2}+n_j^{y2} \le 1 \end{cases}. \tag{34}$$

Differential coefficients of $\hat{\boldsymbol{t}}_{1,k}$, $\hat{\boldsymbol{t}}_{2,k}$, and $\hat{\boldsymbol{t}}_{3,k}$ are expressed using $L_k = ||\boldsymbol{X}_{j+1} - \boldsymbol{X}_j||$ as

$$\frac{\partial\hat{\boldsymbol{t}}_{1,k}}{\partial u_i} = -\frac{1}{{L_k}^2}\frac{\partial L_k}{\partial u_i}\begin{bmatrix} X_{j+1}^x - X_j^x \\ X_{j+1}^y - X_j^y \\ X_{j+1}^z - X_j^z \end{bmatrix} + \frac{1}{L_k}\begin{bmatrix} \frac{\partial\left(U_{j+1}^x - U_j^x\right)}{\partial u_i} \\ \frac{\partial\left(U_{j+1}^y - U_j^y\right)}{\partial u_i} \\ \frac{\partial\left(U_{j+1}^z - U_j^z\right)}{\partial u_i} \end{bmatrix}, \tag{35}$$

$$\frac{\partial\hat{\boldsymbol{t}}_{2,k}}{\partial u_i} = -\frac{\hat{\boldsymbol{r}}_k\times\hat{\boldsymbol{t}}_{1,k}}{||\hat{\boldsymbol{r}}_k\times\hat{\boldsymbol{t}}_{1,k}||^2}\frac{\partial||\hat{\boldsymbol{r}}_k\times\hat{\boldsymbol{t}}_{1,k}||}{\partial u_i} + \frac{1}{||\hat{\boldsymbol{r}}_k\times\hat{\boldsymbol{t}}_{1,k}||}\frac{\partial\left(\hat{\boldsymbol{r}}_k\times\hat{\boldsymbol{t}}_{1,k}\right)}{\partial u_i}, \tag{36}$$

$$\frac{\partial\hat{\boldsymbol{t}}_{3,k}}{\partial u_i} = -\frac{\hat{\boldsymbol{t}}_{1,k}\times\hat{\boldsymbol{t}}_{2,k}}{||\hat{\boldsymbol{t}}_{1,k}\times\hat{\boldsymbol{t}}_{2,k}||^2}\frac{\partial||\hat{\boldsymbol{t}}_{1,k}\times\hat{\boldsymbol{t}}_{2,k}||}{\partial u_i} + \frac{1}{||\hat{\boldsymbol{t}}_{1,k}\times\hat{\boldsymbol{t}}_{2,k}||}\frac{\partial\left(\hat{\boldsymbol{t}}_{1,k}\times\hat{\boldsymbol{t}}_{2,k}\right)}{\partial u_i}, \tag{37}$$

$$\frac{\partial\hat{\boldsymbol{r}}_k}{\partial u_i} = -\frac{\hat{\boldsymbol{n}}_j+\hat{\boldsymbol{n}}_{j+1}}{||\hat{\boldsymbol{n}}_j+\hat{\boldsymbol{n}}_{j+1}||^2}\frac{\partial||\hat{\boldsymbol{n}}_j+\hat{\boldsymbol{n}}_{j+1}||}{\partial u_i} + \frac{1}{||\hat{\boldsymbol{n}}_j+\hat{\boldsymbol{n}}_{j+1}||}\frac{\partial\left(\hat{\boldsymbol{n}}_j+\hat{\boldsymbol{n}}_{j+1}\right)}{\partial u_i}. \tag{38}$$

Differential coefficients of the independent rotational displacements around $\hat{\boldsymbol{t}}_{1,k}$ and $\hat{\boldsymbol{t}}_{2,k}$ are derived by substituting Eqs. (34)–(38) into Eqs. (32) and (33), respectively.

The rotational displacements are classified into the dependent and independent variables. In the following equations, the nodal rotation angles n_j^R related to element k and $\theta_{3j(k+1)}$ related to element $k+1$, which are connected to node j, are assumed to be independent and dependent variables, respectively. Derivatives of the dependent variable $\theta_{3j(k+1)}$ are computed by differentiating Eqs. (17)–(19), as follows, and using the derivatives of n_j^R and the initial angle α between elements k and $k+1$:

$$\frac{\partial\theta_{3j(k+1)}}{\partial u_i} = \frac{\partial\boldsymbol{f}_3}{\partial u_i}\cdot\hat{\boldsymbol{n}}_j + \boldsymbol{f}_3\cdot\frac{\partial\hat{\boldsymbol{n}}_j}{\partial u_i}, \tag{39}$$

$$\frac{\partial\boldsymbol{f}_3}{\partial u_i} = \frac{\partial\hat{\boldsymbol{t}}_{1,k+1}}{\partial u_i}\times\hat{\boldsymbol{f}}_2 + \hat{\boldsymbol{t}}_{1,k+1}\times\frac{\partial\hat{\boldsymbol{f}}_2}{\partial u_i}, \tag{40}$$

$$\begin{aligned}\frac{\partial\hat{\boldsymbol{f}}_2}{\partial u_i} &= \frac{\partial\hat{\boldsymbol{f}}_1}{\partial u_i}\cos\left(n_j^R+\alpha\right) + \hat{\boldsymbol{f}}_1\left(-\sin\left(n_j^R+\alpha\right)\frac{\partial n_j^R}{\partial u_i}\right) \\ &+ \left(\frac{\partial\hat{\boldsymbol{n}}_j}{\partial u_i}\times\hat{\boldsymbol{f}}_1 + \hat{\boldsymbol{n}}_j\times\frac{\partial\hat{\boldsymbol{f}}_1}{\partial u_i}\right)\sin\left(n_j^R+\alpha\right) \\ &+ \left(\hat{\boldsymbol{n}}_j\times\hat{\boldsymbol{f}}_1\right)\cos\left(n_j^R+\alpha\right)\frac{\partial n_j^R}{\partial u_i},\end{aligned} \tag{41}$$

$$\frac{\partial\hat{\boldsymbol{f}}_1}{\partial u_i} = -\frac{\boldsymbol{f}_1}{||\boldsymbol{f}_1||^2}\frac{\partial||\boldsymbol{f}_1||}{\partial u_i} + \frac{1}{||\boldsymbol{f}_1||}\frac{\partial\boldsymbol{f}_1}{\partial u_i}, \tag{42}$$

$$\frac{\partial\boldsymbol{f}_1}{\partial u_i} = \frac{\partial\hat{\boldsymbol{t}}_{1,k}}{\partial u_i} - \left[\left(\frac{\partial\hat{\boldsymbol{t}}_{1,k}}{\partial u_i}\cdot\hat{\boldsymbol{n}}_j + \hat{\boldsymbol{t}}_{1,k}\cdot\frac{\partial\hat{\boldsymbol{n}}_j}{\partial u_i}\right)\hat{\boldsymbol{n}}_j + \left(\hat{\boldsymbol{t}}_{1,k}\cdot\hat{\boldsymbol{n}}_j\right)\frac{\partial\hat{\boldsymbol{n}}_j}{\partial u_i}\right]. \tag{43}$$

If node j is a rigid support, then differential coefficients of rotational displacements around unit normal vectors are computed as:

$$\frac{\partial\theta_{3jk}}{\partial u_i} = \frac{\partial\boldsymbol{g}_1}{\partial u_i}\hat{\boldsymbol{n}}_j + \boldsymbol{g}_1\frac{\partial\hat{\boldsymbol{n}}_j}{\partial u_i}, \tag{44}$$

$$\frac{\partial\boldsymbol{g}_1}{\partial u_i} = \frac{\partial\hat{\boldsymbol{t}}_{1,k}}{\partial u_i}\times\hat{\boldsymbol{t}}_{1,k}^* + \hat{\boldsymbol{t}}_{1,k}\times\frac{\partial\hat{\boldsymbol{t}}_{1,k}^*}{\partial u_i}. \tag{45}$$

5. Artificial mass, inertia moment, and damping

Artificial mass and inertia moment are to be assigned to compute the dynamic responses using Eq. (1). The general stiffness S_k is defined as EA/L_k for translation and $EI/{L_k}^3$ for rotation. Suppose node j is connected by $q(\geq 1)$ element(s) which is/are

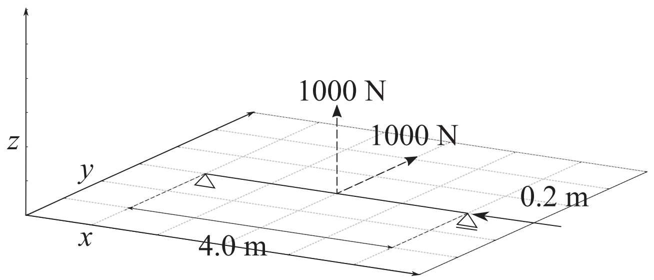

Fig. 7. Initial shape and boundary conditions of the simple beam model (arrow at the roller-support: forced displacement of 0.20 m, dashed arrows: external force of 1000 N in positive y- and z-directions).

not limited to be collinear. We use the approach formulated by Lefevre et al. (2017) to compute the artificial mass/inertia moment at node j, which is formulated using a weight parameter γ as

$$M_j = \gamma \, \Delta t_{\mathrm{ini}}{}^2 \sum_{k=1}^{q} 2^n S_k. \tag{46}$$

where n is a parameter; if S_k represents the translational stiffness, $n = 1$; otherwise, $n = 3$. Note that S_k should be appropriately scaled if the members are diagonally connected.

If the element lengths become smaller, then the artificial mass and inertia moment become larger, and convergence property of the DRM is deteriorated; i.e., we need many iterations if there are short elements. Therefore, we have to find the value of the weight parameter γ corresponding to the appropriate values of the artificial mass and inertia moment satisfying the Courant–Friedrichs–Lewy condition for determining the time increment for an explicit integration method. Using the artificial mass/inertia moment at node j, and the summation of the general stiffness S_k of the elements connected to node j, the Courant–Friedrichs–Lewy condition can be formulated as:

$$\frac{\Delta t_{\mathrm{ini}}{}^2 \sum_{k=1}^{q} S_k}{M_j} < 2. \tag{47}$$

The DRM cannot arrive at the static equilibrium state without any damping, as is the case with general vibration problems. Therefore, an artificial damping is usually assigned in DRM. There are two types of artificial damping: viscous damping and kinetic damping. The former is used for directly reducing velocity vectors utilizing viscous damping matrix. We use the latter, which resets the kinetic energy to 0 after obtaining its local peak as described in Step 6 of the DRM algorithm. In this case, there is no damping matrix, and the acceleration vector is computed from Eq. (5). The velocity vector is also reset as

$$\boldsymbol{v}^{t+\Delta t/2} = \frac{\Delta t}{2} \boldsymbol{M}^{-1} \boldsymbol{R}^t. \tag{48}$$

6. Numerical examples

The proposed DRM is applied to large-deformation analysis for generating forms of elastic gridshells. The expressions of the residual forces are also implemented in the optimization method to minimize the total potential energy Π_{total}, where the quasi-Newton method in the library of SNOPT Ver. 7 (Gill et al., 2002) is used for solving the unconstrained optimization problem. In the algorithm of DRM, step size Δt is updated as $0.9969\Delta t$ after reaching a kinetic energy peak, i.e., $\xi = 0.9969$ in Step 7 of the DRM algorithm. The value of $\xi = 0.9969$ is chosen by carrying out preliminary analyses to require the smallest the number of steps to satisfy convergence criterion. The weight parameter γ in Eq. (46) is 0.8. In addition, FEM by Abaqus Ver. 2016 (Systèmes, 2016) is carried out for verification of the shapes obtained by the proposed method. The loading parameter t_{FEM} for FEM is increased from 0.0 to 2.0 with the maximum time increment 5.0×10^{-4}. In the period $0.0 \le t_{\mathrm{FEM}} \le 1.0$, the upward virtual

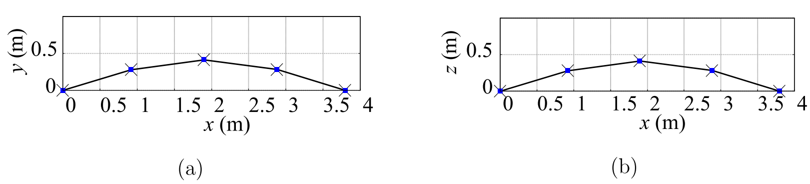

Fig. 8. Equilibrium shape of simple beam model; (a) xy-plane, (b) xz-plane (cross: FEM, line: DRM, square: optimization).

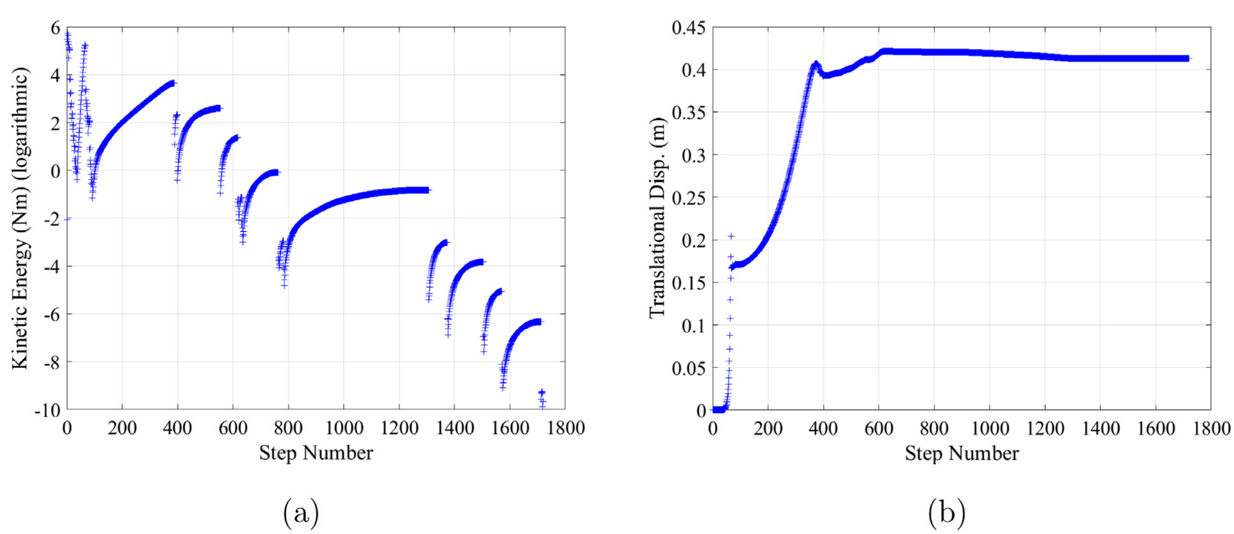

Fig. 9. Iteration histories of kinetic energy and displacement; (a) kinetic energy of all nodes, (b) translational displacement in z-direction of the center node.

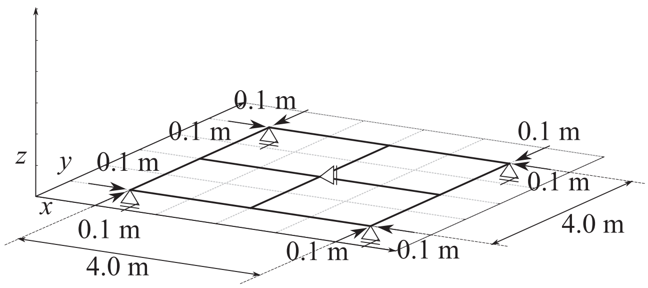

Fig. 10. Initial shape and boundary conditions of the short span gridshell (arrows at four corners: forced displacement of 0.10 m).

load equal to self-weight is applied to all members linearly in order to avoid the numerical difficulty due to bifurcation buckling at the initial deformation from the flat grid to the curved surface. During the period $1.0 \leq t_{FEM} \leq 2.0$, we apply the forced displacements and the external loads to obtain the final equilibrium shape while reducing the upward virtual load to 0.

In the following examples, we use a material with Young's modulus 200 GPa and Poisson's ratio 0.3. The beam has a pipe section with diameter $d_d = 0.030$ m and thickness $d_t = 0.002$ m. The initial length of each beam element is $l = 1.00$ m; accordingly, the slenderness ratio of each element is $100.76(= 4l/\sqrt{{d_d}^2 + (d_d - 2d_t)^2})$. Computation is carried out on a PC with Intel Core i7-8700 CPU 3.20 GHz, 16.0GB RAM and six cores.

6.1. Simple beam model

A simple slender beam model, which is unstressed and straight in the initial state, is arranged along x-axis. The model has five nodes, pin-supported at one end, and roller-supported at the other end allowing translational displacement in x-direction. Note that the rotations around x-axis are also constrained at the both end nodes for FEM. In the optimization method, the ranges of the variables such as U_j^x, U_j^y, U_j^z, n_j^x, n_j^y, and n_j^R are specified as $[-1.0, 1.0]$.

Table 1
Maximum and average differences of the coordinates of all nodes between DRM and FEM of three models.

		x (m)	y (m)	z (m)
Simple beam model	Maximum	2.110×10^{-4}	4.013×10^{-4}	5.265×10^{-4}
	Average	8.441×10^{-5}	2.318×10^{-4}	2.208×10^{-4}
Short span gridshell	Maximum	2.567×10^{-3}	2.568×10^{-3}	2.141×10^{-3}
	Average	3.878×10^{-4}	3.878×10^{-4}	7.013×10^{-4}
Long span gridshell	Maximum	1.255×10^{-4}	1.255×10^{-4}	9.916×10^{-4}
	Average	3.644×10^{-5}	3.644×10^{-5}	2.974×10^{-4}

We apply external loads of 1000 N in y- and z-directions at the center node. A forced displacement of - 0.20 m is applied in x-direction at the roller-support. Fig. 7 shows the initial shape and the boundary conditions of the simple beam model. Fig. 8(a) and (b) show the equilibrium shapes of simple beam model in xy- and xz-plane, respectively. The results of the DRM, the optimization method, and the FEM are very close, as shown in Fig. 8. The total potential energy resulting from the DRM and the optimization method are - 367.933 Nm and - 367.931 Nm, respectively, which are very close. The number of steps of DRM and the optimization method are 1720 and 860, respectively. Note that the same process of sensitivity analysis in Section 4 is carried out at each step of the DRM and the optimization method. However, approximate Hessian of the total potential energy is computed in the optimization method, which requires additional computational cost.

Fig. 9(a) and (b) show the iteration histories of the total kinetic energy and the z-directional displacement of the center node, respectively, obtained by the DRM. Although the total number of steps is very large, an approximate solution is found about half of the total steps.

Table 1 shows the maximum and average differences in x-, y-, and z-coordinates of all nodes between DRM and FEM. The maximum difference in z-direction is 5.265×10^{-4} m, which is very small.

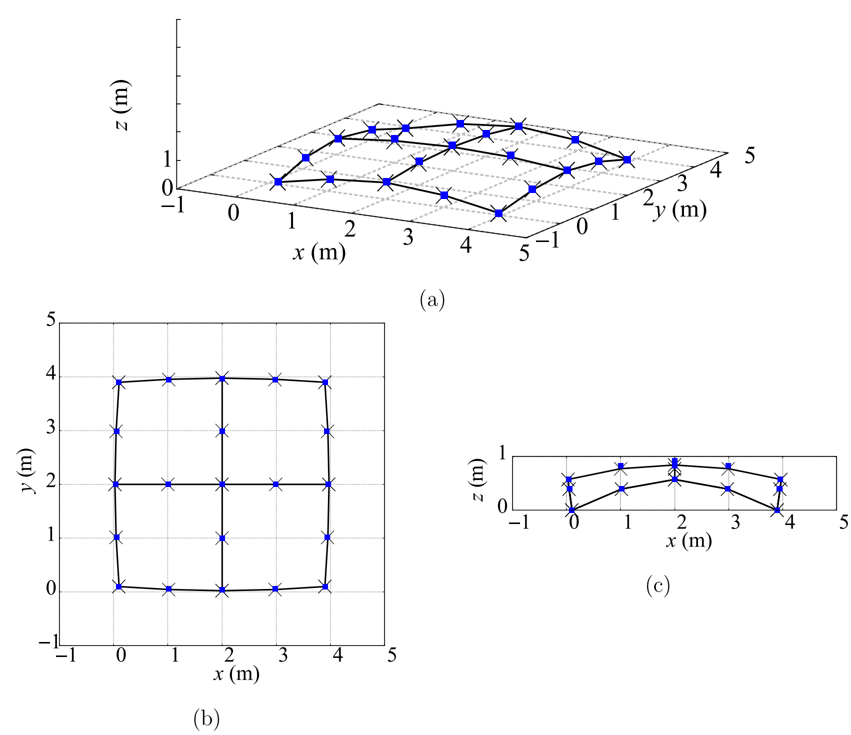

Fig. 11. Short span gridshell; (a) equilibrium shape, (b) xy-plane, (c) xz-plane (cross: FEM, line: DRM, square: optimization).

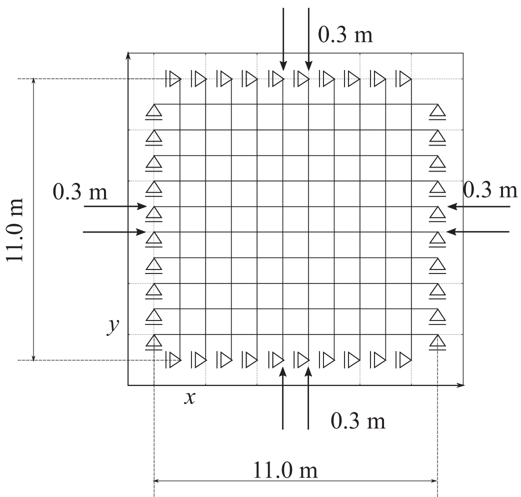

Fig. 12. Initial shape and boundary conditions of long span gridshell (arrow: forced displacement of 0.30 m).

6.2. Short span gridshell

Consider a gridshell which has a 4 × 4 (m) square boundary and two internal beams intersecting at the center. The model has six beams, each of which is divided into four elements. The nodes at $(x, y, z) = (0, 0, 0)$, (4,0,0), (0,4,0), and (4,4,0) have roller supports that can move in x- and y-directions. The center node at (2,2,0) has a roller support that can move in z-direction only. Note that rotations around the three axes are also constrained at the center to ensure symmetric deformation.

Forced displacements of $\sqrt{2}/10$ m are applied at the four corner supports toward the center node (2,2,0). Fig. 10 shows the initial shape and the boundary conditions of the short span gridshell. The equilibrium shapes obtained by the DRM, the optimization method, and the FEM are close as shown in Fig. 11. The total potential energy resulting from the DRM and the optimization method are 2.214 kNm and 2.320 kNm, respectively, which are close. The number of steps of DRM and the optimization method are 3410 and 1845, respectively. In the optimization method, the ranges of the variables U_j^x, U_j^y, and U_j^z are specified as $[-1.5, 1.5]$, and those for n_j^x, n_j^y, and n_j^R are $[-1.0, 1.0]$. The maximum and average differences in x-, y-, and z-coordinates of all nodes between the DRM and the FEM are listed in Table 1. The maximum difference in y-coordinates is 2.568×10^{-3} m, which is larger than that of long span gridshell in the next section. However, the value is still less than 1/300 of the element length, and is negligible in practical applications.

6.3. Long span gridshell

Consider a long span gridshell composed of 20 beams that have the same length 11.00 m, which are classified into two groups with ten beams in x- and y-directions, respectively. All beams are roller supported at both ends in the longitudinal direction of the beam. In the optimization method, the ranges of the variables U_j^x, U_j^y, and U_j^z are specified as $[-2.0, 2.0]$, and those for n_j^x, n_j^y, and n_j^R are $[-1.0, 1.0]$. Fig. 12 shows the initial shape and the boundary conditions of the long span gridshell.

Fig. 13 shows the equilibrium shape obtained by the DRM, the optimization method, and the FEM, which are very close. The total potential energy resulting from the DRM and the optimization method are 2.763 kNm and 3.870 kNm. The number of steps of DRM and the optimization method are 8449 and 6375, respectively. The maximum and average differences of x-, y-, and z-coordinates of all nodes between the DRM and the FEM are listed in Table 1. The maximum difference in z-direction is 9.916×10^{-4} m, which is very small.

7. Conclusions

The main purpose of this study is to propose a 3-dimensional elastic beam model for large-deformation analysis of elastic grid-

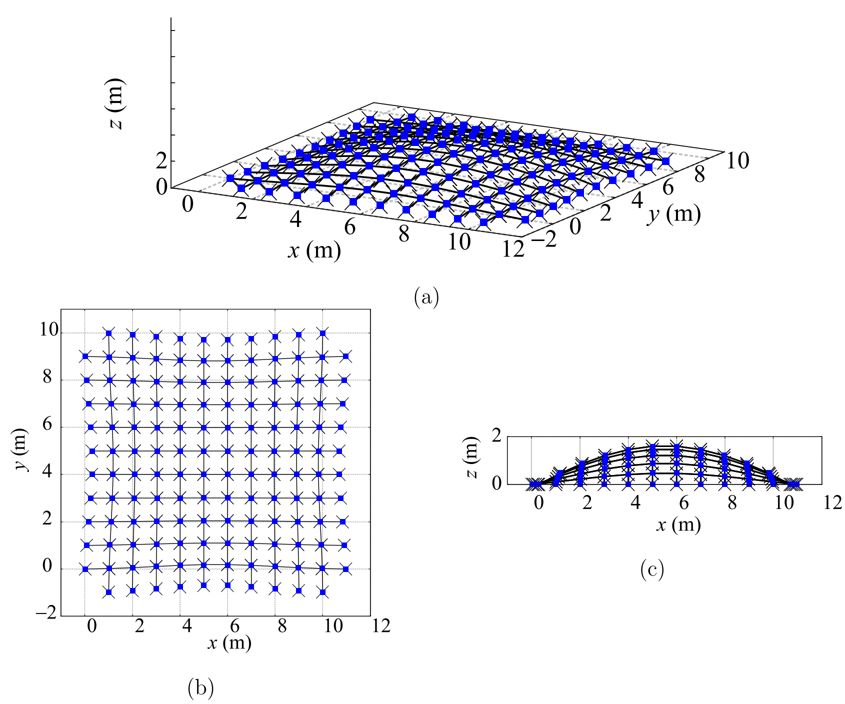

Fig. 13. Long span gridshell; (a) equilibrium shape, (b) xy-plane, (c) xz-plane (cross: FEM, line: DRM, square: optimization).

shells using the DRM. The residual nodal forces at a deformed state are derived by differentiating the total potential energy with respect to the generalized displacement components. Since the DRM solves the dynamic equilibrium equations explicitly, incremental form of equilibrium equations and the tangent stiffness matrix need not be derived. The proposed formulation can also be applied to an optimization approach for directly minimizing the total potential energy.

In the proposed formulation, the unit normal vector of a curved surface of gridshell at each node is used for obtaining the local deformation. Six independent variables at a node consist of the three translational displacements, two horizontal components of the unit normal vector, which are reduced to the two components representing the inclination of the unit normal vector from the local member axes, and the rotation around the unit normal vector at the deformed state. Bending and torsional deformations at the two end nodes are computed by using the geometrical relationships between the unit normal vector at each node and orientations of local element axes. The total potential energy is formulated at the deformed state, and the residual forces are derived by differentiating the total potential energy with respect to the generalized displacement components. Therefore, our formulation does not require incremental form of large rotation, and does not have any difficulty involved in the co-rotational formulation of the beam elements.

Since the residual forces are equivalent to the differential coefficients of the total potential energy in the framework of optimization method, the deformed equilibrium state is also obtained using an optimization method. In the numerical examples, we compared the solutions obtained by the DRM, optimization, and FEM for three models. It is important to develop a simple method of DRM that is readily available to the designers, because the general designers cannot have access to sophisticated optimization library and/or FEM software package. In all models, the deformed shapes obtained by the DRM and optimization are almost equal to the shape obtained by an FEM software package. This result suggests that 3-dimensional elastic beam model described by the unit normal vectors can be effectively applied to form-finding of elastic gridshells.

Declaration of Competing Interest

The authors declare that they have no known competing financial interests or personal relationships that could have appeared to influence the work reported in this paper.

Acknowledgment

This research is partly supported by SPIRITS program 2017 of Kyoto University.

References

Adriaenssens, S., Barnes, M., Harris, R., Williams, C., 2004. Dynamic relaxation: design of a strained timber gridshell. In: Adriaenssens, S., Block, P., Veenendaal, D., Williams, C. (Eds.), Shell Structures for Architecture. Routledge, London, pp. 89–102. doi:10.4324/9781315849270.

Adriaenssens, S.M.L., Barnes, M.R., 2001. Tensegrity spline beam and grid shell structures. Eng. Struct. 23 (1), 29–36. doi:10.1016/S0141-0296(00)00019-5.

Barnes, M., Adriaenssens, S., Krupka, M., 2013. A novel torsion/bending element for dynamic relaxation modeling. Eng. Struct. 119, 60–67. doi:10.1016/j.compstruc.2012.12.027.

Bel Hadj Ali, N., Rhode-Barbarigos, L., Smith, I.F.C., 2011. Analysis of clustered tensegrity structures using a modified dynamic relaxation algorithm. Int. J. Solids Struct. 48, 637–647. doi:10.1016/j.ijsolstr.2010.10.029.

Bel Hadj Ali, N., Sychterz, A.C., Smith, I.F.C., 2017. A dynamic-relaxation formulation for analysis of cable structures with sliding-induced friction. Int. J. Solids Struct. 126-127 240–251. doi:10.1016/j.ijsolstr.2017.08.008.

Belytschko, T., Hsieh, B.J., 1973. Non-linear transient finite element analysis with convected co-ordinates. Int. J. Numer. Meth. Eng. 7, 255–271. doi:10.1002/nme.1620070304.

Bessini, J., Lázaro, C., Monleón, S., 2017. A form-finding method based on the geometrically exact rod model for bending-active structures. Eng. Struct. 152 (1), 549–558. doi:10.1016/j.engstruct.2017.09.045.

Cardona, A., Géradin, M., 1988. A beam finite element non-linear theory with finite rotations. Int. J. Numer. Meth. Eng. 26, 2403–2438. doi:10.1002/nme.1620261105.

Crisfield, M.A., 1990. A consistent co-rotational formulation for non-linear, three-dimensional, beam-elements. Comput. Method. Appl. M. 81, 131–150. doi:10.1016/0045-7825(90)90106-V.

D'Amico, B., Kermani, A., Zhang, H., 2014. Form finding and structural analysis of actively bent timber grid shells. Eng. Struct. 81, 195–207. doi:10.1016/j.engstruct.2014.09.043.

D'Amico, B., Kermani, A., Zhang, H., Shepherd, P., Williams, C.J.K., 2015. Optimization of cross-section of actively bent grid shells with strength and geometric compatibility constraints. Comput. Struct. 154, 163–176. doi:10.1016/j.compstruc.2015.04.006.

D'Amico, B., Zhang, H., Kermani, A., 2016. A finite-difference formulation of elastic rod for the design of actively bent structures. Eng. Struct. 117, 518–527. doi:10.1016/j.engstruct.2016.03.034.

Day, A.S., 1965. An introduction to dynamic relaxation. The Engineer 219, 218–221.

Gill, P.E., Murray, W., Saunders, M.A., 2002. SNOPT: an SQP algorithm for large-scale constrained optimization. SIAM. J. Opt. 12, 979–1006. doi:10.1137/S0036144504446096.

Happold, E., Liddell, W.I., 1975. Timber lattice roof for the mannheim bundesgartenschau. Struct. Eng. 53 (3), 99–135. https://www.scopus.com/inward/record.uri?eid=2-s2.0-0016484016&partnerID=40&md5=aba8fcc81e1470558686 86db675ec892.

Harris, R., Romer, J., Kelly, O., Johnson, S., 2003. Design and construction of the downland gridshell. Build. Res. Inf. 31 (6), 427–454. doi:10.1080/0961321032000088007.

Hsiao, K.M., 1992. Co-rotational total lagrangian formulation for three-dimensional beam element. AIAA. J. 30 (3), 797–804. doi:10.2514/3.10987.

Ibrahimbegović, A., 1995. On finite element implementation of geometrically nonlinear Reissner's beam theory: three-dimensional curved beam elements. Comput. Meth. Appl. Mech. Eng. 122, 11–26. doi:10.1016/0045-7825(95)00724-F.

Krenk, S., 2009. Nonlinear Modeling and Analysis of Solids and Structures. Cambridge University Press, Cambridge doi:10.1017/CBO9780511812163.

Lázaro, C., Bessini, J., Monleón, S., 2018. Mechanical models in computational form finding of bending-active structures. Int. J. Sp. Struct. 33, 86–97. doi:10.1177/0266351118794277.

Lefevre, B., Tayeb, F., du Peloux, L., Caron, J.F., 2017. A 4-degree-of-freedom kirchhoff beam model for the modeling of bending-torsion couplings in active-bending structures. Int. J. Sp. Struct. 32, 69–83. doi:10.1177/0266351117714346.

Li, J.M., Knippers, J., 2012. Rotational formulations for dynamic relaxation - with application in 3d framed structures with large displacements and rotations. In: Proc. IASS-APCS 2012. Seoul, Korea, Paper No. FF-157

Li, Z.X., Vu-Quoc, L., 2010. A mixed co-rotational 3d beam element formulation for arbitrarily large rotations. Adv. Steel. Constr. 6 (2), 767–787. http://ascjournal.com/down/vol6no2/vol6no2_7.pdf

Nielsen, M.B., Krenk, S., 2014. Eplicit free-floating beam element. Int. J. Numer. Meth. Eng. 98, 59–78. doi:10.1002/nme.4623.

Reissner, E., 1972. On one-dimensional finite-strain beam theory: the plane problem. J. Appl. Math. Phys. 23 (5), 795–804. doi:10.1007/BF01602645.

Rombouts, J., Lombaert, G., De Laet, L., Schevenels, M., 2018. On the equivalence of dynamic relaxation and the Newton-Raphson method. Int. J. Numer. Meth. Eng. 113, 1531–1539. doi:10.1002/nme.5707.

Rombouts, J., Lombaert, G., De Laet, L., Schevenels, M., 2019. A novel shape optimization approach for strained gridshells: Design and construction of a simply supported gridshell. Eng. Struct. 192 (1), 166–180. doi:10.1016/j.engstruct.2019.04.101.

Sakai, Y., Ohsaki, M., 2018. Discrete elastica for shape design of gridshells. Eng. Struct. 169. doi:10.1016/j.engstruct.2018.05.002.

Senatore, G., Piker, D., 2015. Interactive real-time physics: An intuitive approach to form-finding and structural analysis for design and education. CAD Comput. Aided Des. 61, 32–41. doi:10.1016/j.cad.2014.02.007.

Simo, J., 1985. A finite strain beam formulation. the three-dimensional dynamic problem. Part I. Comput. Meth. Appl. Mech. Eng. 49 (1), 55–70. doi:10.1016/0045-7825(85)90050-7.

Simo, J.C., Vu-Quoc, L., 1986. A three-dimensional finite-strain rod model, part II: Computational aspects. Comput. Methods Appl. Mech. Eng. 58, 79–116. doi:10.1016/0045-7825(86)90079-4.

Simo, J.C., Vu-Quoc, L., 1991. A geometrically exact rod model incorporating shear and torsion-warping deformation. Int. J. Solids. Struct. 27 (3), 371–393. doi:10.1016/0020-7683(91)90089-X.

Sonneville, V., Cardona, A., Bruls, O., 2014. Geometrically exact beam finite element formulated on the special euclidean group SE(3). Comput. Meth. Appl. Mech. Eng. 268, 451–474. doi:10.1016/j.cma.2013.10.008.

Systèmes, D., 2016. Abaqus user's manual ver. 2016. http://127.0.0.1:2080/v2016/.